JCTC Journal of Chemical Theory and Computation

ARTICLE

pubs.acs.org/JCTC

Introduction of a New Theory for the Calculation of Magnetic Coupling Based on Spin−Flip Constricted Variational Density Functional Theory. Application to Trinuclear Copper Complexes which Model the Native Intermediate in Multicopper Oxidases

Hristina Zhekova, Michel Seth, and Tom Ziegler*

Department of Chemistry, University of Calgary, Calgary, Alberta Canada T2N 1N4

ABSTRACT: We have introduced a new method for the calculation of spin−exchange between weakly interacting electron spins on different metal centers. The method is based on spin−flip constricted variational density functional theory (SF-CV-DFT). The application of SF-CV-DFT to two trinuclear systems $[Cu_3(L)(\mu_3{-}O)]^{4+}$ and $[(L')_3]Cu_3(\mu{-}OH)_3]^{3+}$ revealed that SF-CV-DFT affords exchange coupling constants that are similar to the values obtained by the traditional broken-symmetry (BS) scheme for the same functional. The BHandHLYP functional affords for both systems the best fit to experiment and results from high-level theory in the case of BS-DFT as well as SF-CV(2)-DFT. All methods and functionals predict $[Cu(L)(\mu_3{-}O)]^{4+}$ to be ferromagnetic and the $[(L')_3Cu_3(\mu{-}OH)_3]^{3+}$ system to be antiferromagnetic. The SF-CV(2)-DFT method is not only able to evaluate exchange coupling constants, it can in addition calculate the full multiplet spectrum with complete use of spatial symmetry. Further, in its restricted formulation, calculations can be carried out with use of full spin−symmetry without spin−contamination.

1. INTRODUCTION

The two trinuclear copper complexes of the present study, $[Cu(L)(\mu_3{-}O)]^{4+}$ (where L is a complex dodecaaza macrotetracycle)[1] and $[(DBED)_3Cu_3(\mu{-}OH)_3]^{3+}$ (where DBED stands for *N,N′*-ditert-butyl-ethylenediamine),[2] have attracted considerable attention as synthetic analogues of the native intermediate (NI) occurring during the catalytic reactions at the active sites of the multicopper oxidases.[3−5] The latter is a metalloenzyme found in some plants, fungi and animals and involved in the four e^- reduction of O_2 to H_2O.[6−8] The reduction process is coupled with four one-electron oxidations of a substrate and leads to the synthesis of key metabolite substances of vital importance. Some of the most studied multicopper oxidases are laccase,[9] ascorbate oxidase,[10] ceruloplasmin,[11] and Fet3p.[12]

Two potential models of NI,[1,2] $[Cu_3(L)(\mu_3{-}O)]^{4+}$ and $[(DBED)_3Cu_3(\mu{-}OH)_3]^{3+}$, were synthesized and studied extensively with X-ray diffraction, magnetic susceptibility, absorption spectroscopy, electron paramagnetic resonance (EPR), and conventional and ariable-temperature, variable-fieldmagnetic circular dichroism (VTVH MCD).[1−5] $[Cu_3(L)(\mu_3{-}O)]^{4+}$ was found to be ferromagnetic with a quartet ^4A ground state and a low-lying doublet ^2E excited state situated 163.5 cm^{-1} above the ground state.[1,3] The second structure, $[(DBED)_3Cu_3(\mu{-}OH)_3]^{3+}$ is antiferromagnetic[2,4] and has a doublet ^2E ground state and a quartet $^4A_1$ excited state with a $^2E - {}^4A_1$ energy gap of 315 cm^{-1}. The VTVH MCD studies[5,13] point to the $[Cu_3(L)(\mu_3{-}O)]^{4+}$ model as the one that best reproduces the observed MCD spectrum of NI.

The ground and the lowest excited states of the two synthetic models were analyzed theoretically with density functional theory (DFT)[3−5,13] and multireference complete active space second-order perturbation theory/complete active space self-consistent field (CASPT2/CASSCF) and multireference difference dedicated CI 2-degrees of freedom (MRDDCI2) methods.[14−17] The DFT calculations employed the broken symmetry approach[18] for the simulation of the doublet states in C_3 and D_3 symmetry for $[Cu_3(L)(\mu_3{-}O)]^{4+}$ and $[(DBED)_3Cu_3(\mu{-}OH)_3]^{3+}$, respectively. CASPT2/CASSCF calculations with and without spin−orbit coupling corrections were done[16] in order to estimate the quartet−doublet splitting for $[Cu_3(L)(\mu_3{-}O)]^{4+}$ and $[(DBED)_3Cu_3(\mu{-}OH)_3]^{3+}$ in C_s and C_2 symmetry, respectively. These results were then correlated to the structures in their original symmetry (C_3 and D_3, respectively). The CASPT2/CASSCF studies afford good agreement with the experimental data with regard to spin multiplicity and the relative energy of the ground and low-lying excited states.[16,17]

The multireference methods, albeit more accurate than DFT, are computationally expensive and difficult to apply for systems larger than 40 atoms. On the other hand, conventional DFT, which is a good compromise between accuracy and model size, has problems in describing some of the open shell spin states encountered in the two model systems discussed here. The difficulties arise from the fact that conventional DFT as a single determinantal method has problems with the description of spin states that even to zero order must be represented by a multideterminantal wave function.[18,19]

This problem is partially circumvented within the conventional DFT formalism by the broken symmetry method,[18] where use is made of a simple Heisenberg Hamiltonian.[20] The single determinantal broken symmetry state is represented as a weighted average of the pure spin states of a system. The difference of the energy of the broken symmetry states and the

Received: February 25, 2011
Published: May 05, 2011

pure symmetry state of highest spin (which can be described easily by a single determinant) can be related directly to the exchange coupling constants J_{ij} of the Heisenberg Hamiltonian[18] and hence to the difference in energy of the various spin states. This approach is straightforward and computationally feasible. However it does not provide detailed separate information about each individual spin state aside from their relative energies.

Time-dependent density functional theory (TDDFT)[21,22] is in contrast to conventional DFT and is able to describe states of a multideterminantal nature as "excited states" relative to a single determinantal reference. In conventional TDDFT this reference is the ground state. However based on the constricted variational DFT (CV-DFT) formulation[23] of the reference can be any state. We shall in the following demonstrate that we can describe the different spin states in our two model compounds with the help of CV-DFT using the pure symmetry state of highest spin as a reference. As some of the spin states are related to the reference by spin−flip, we will make use of spin−flip theory[24] based on our noncollinear exchange−correlation potential formulation[25−27] as implemented into the Amsterdam Density Functional (ADF) package.[28,29] It is the objective of the present investigation to apply the novel spin−flip CV-DFT scheme[23] to the difference in energy of the various spin states encountered in the two model systems $[Cu_3(L)(\mu_3{-}O)]^{4+}$ and $[(DBED)_3Cu_3(\mu{-}OH)_3]^{3+}$. We hope in addition to provide the first test of the novel spin−flip CV-DFT scheme as an alternative to the broken symmetry method[18] in DFT-based studies of magnetic coupling between weakly interacting metal centers.

2. COMPUTATIONAL METHODS AND DETAILS

Formulation of the CV-DFT to Second Order. We shall in accordance with Kohn−Sham (KS) theory[19] describe our reference state by a single Slater determinant:

$$\Psi^0 = |\psi_1\psi_2\ ,\ ...,\ \psi_i\psi_j\ ,\ ...,\ \psi_n| \tag{1}$$

constructed from a set of occupied spin−orbitals $\{\psi_i(1);\ i = 1,\text{occ}\}$ The related density matrix[19] is given by

$$\rho(1,1') = \sum_i^{\text{occ}} \psi_i^*(1')\psi_i(1) \tag{2}$$

The energy of the reference system corresponding to the density matrix in eq 2 can be expressed as

$$\begin{aligned} E_{KS} &= E_{T+V_{Ne}} + E_C + E_{XC,KS} \\ &= \int [\hat{h}^0(1')\rho(1,1')]_{(1=1')}d\tau_1 + \frac{1}{2}\int \rho(1,1)\frac{1}{r_{12}}\rho(2,2)d\tau_1 d\tau_2 \\ &\quad + \int E_{XC,KS}[\rho(1,1)]d\tau_1 \end{aligned} \tag{3}$$

The one-electron Hamiltonian $\hat{h}^0$ includes the kinetic energy operator $(\hat{T})$ for a single electron and the potential (V_{Ne}) from the nuclear-electron interactions. E_C represents the coulomb interactions of the molecular electron density with itself. $E_{XC,KS}$ is the exchange−correlation energy, defined as a functional of the electron density $\rho(1,1)$.

The spin−orbitals $\{\psi_i(1);\ i = 1,\text{occ}\}$ of eq 1 that afford the minimum energy according to eq 3, satisfy the one-electron KS equation:

$$\hat{F}^{KS}(1)\psi_i(1) = \varepsilon_i\psi_i(1) \tag{4}$$

with the KS operator $\hat{F}^{KS}$ defined as

$$\hat{F}^{KS}(1) = \hat{h}^0 + \int \rho(2,2)\frac{1}{r_{12}}d\tau_2 + V_{XC}(1) \tag{5}$$

Here

$$V_{XC}[\rho] = \frac{\delta E_{XC}}{\delta\rho} \tag{6}$$

is the exchange−correlation potential expressed as the functional derivative of the exchange−correlation energy with respect to the density.

The solution of eq 4 yields a set of optimized occupied $\{\psi_i(1);\ i = 1,\text{occ}\}$ and virtual $\{\psi_a(1);\ a = 1,\text{vir}\}$ spin orbitals. Given that the complete set of spin orbitals $\{\psi_p(1);\ p = 1,\text{occ} + \text{vir}\}$ are solutions to eq 4, we can write

$$F_{rs}^{KS} = \int \psi_r^*(1)\hat{F}^{KS}(1)\psi_s(1)d\tau_1 = \delta_{rs}\varepsilon_r \tag{7}$$

In CV-DFT[23] we seek new determinantal wave functions:

$$\Psi' = |\psi'_1\psi'_2\ ,\ ...,\ \psi'_i\psi'_j\ ,\ ...,\ \psi'_n| \tag{8}$$

that ultimately will represent excited states. Here the orbital set $\{\psi'_i(1);\ i = 1,\text{occ}\}$ in eq 8 is constructed by mixing into each of the occupied reference orbitals $\{\psi_i(1);\ i = 1,\text{occ}\}$ a fraction of the virtual reference orbitals $\{\psi_a(1);\ a = 1,\text{vir}\}$:

$$\delta\psi_i = \sum_a^{\text{vir}} U_{ai}\psi_a \tag{9}$$

where the mixing coefficient U_{ai} shall serve as a variational parameter that minimizes the energy associated with the excited state that is represented by Ψ'.

After orthonormalization to second order in U, we can write the new set of occupied orbitals as

$$\psi'_i(1) = \psi_i(1) + \sum_a^{\text{vir}} U_{ai}\psi_a(1) - \frac{1}{2}\sum_a^{\text{vir}}\sum_k^{\text{occ}} U_{ai}U_{ak}^*\psi_k(1) + O^{(3)}[U] \tag{10}$$

The density matrix corresponding to ψ' of eq 8 now reads to second order in U:

$$\begin{aligned} \rho'(1,1') &= \rho(1,1') + \Delta\rho'(1,1') = \rho(1,1') \\ &\quad + \sum_i^{\text{occ}}\sum_a^{\text{vir}} U_{ai}^*\psi_{ai}^*(1)\psi_a(1') + \sum_i^{\text{occ}}\sum_a^{\text{vir}} U_{ai}^*\psi_a^*(1)\psi_i(1') \\ &\quad + \sum_a^{\text{vir}}\sum_b^{\text{vir}}\sum_i^{\text{occ}} U_{ai}^*U_{bi}\psi_a^*(1)\psi_b(1') \\ &\quad - \sum_i^{\text{occ}}\sum_k^{\text{occ}}\sum_a^{\text{vir}} U_{ak}^*U_{ai}\psi_i^*(1)\psi_k(1') + O^{(3)}[U] \end{aligned} \tag{11}$$

A substitution of eq 11 into eq 3 affords[23] the energy of Ψ' to second order in U as

$$\begin{aligned} E_{KS}[\rho^0 + \Delta\rho'] - E_{KS}[\rho^0] &= \Delta E_{KS}[\Delta\rho'] + O^{(3)}[U] \\ &= \frac{1}{2}(U^*\ U)\begin{pmatrix} \mathbf{A}^{KS} & \mathbf{B}^{KS} \\ \mathbf{B}^{KS} & \mathbf{A}^{KS} \end{pmatrix}\begin{pmatrix} U \\ U^* \end{pmatrix} + O^{(3)}[U] \end{aligned} \tag{12}$$

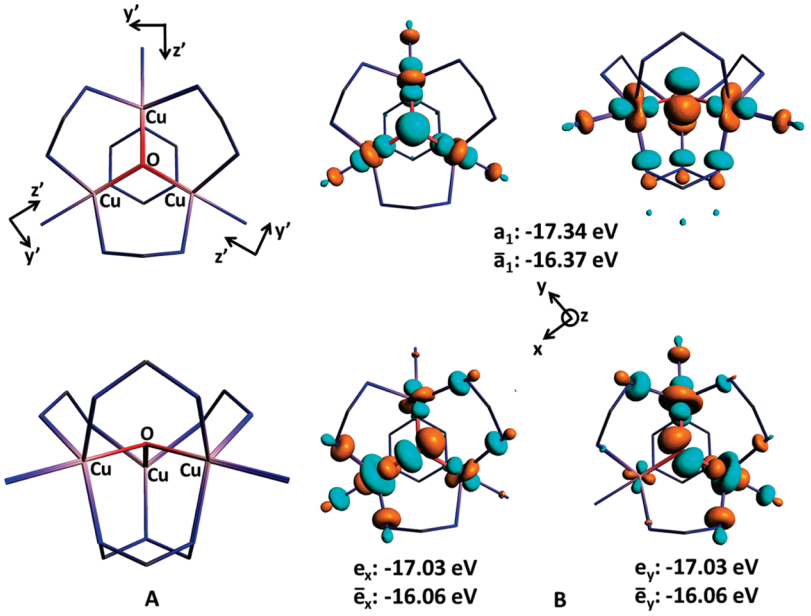

Figure 1. (A)The μ_3O model in C_{3V} symmetry: front view (up) and side view (down). Included are the copper centered coordinate systems x',y',z'. (B) Frontier SUMO orbitals of $(\mu_3O)_{C_{3v}}$. Up: Front and side view of $\bar{a}_1$, along with the values of the orbital energies. Down: Front view of the $\bar{e}_x$ and $\bar{e}_y$ orbitals with the orbital energies and the orientation of the molecular coordinate system x,y,z. The SOMO orbitals a_1, e_x, and e_y are not shown, since they have similar spatial distribution as their SUMO counterparts.

The 2×2 supermatrix in eq 12 is also known as the electronic ground-state Hessian. Its matrix elements $A^{KS}_{ai,bj}$ and $B^{KS}_{ai,bj}$ of $\mathbf{A^{KS}}$ and $\mathbf{B^{KS}}$, respectively, are given by

$$A^{KS}_{ai,\,bj} = \delta_{ab}\delta_{ij}(\varepsilon_a - \varepsilon_i) + K^{KS}_{ai,\,bj}; B^{KS}_{ai,\,bj} = K^{KS}_{ai,\,jb} \qquad (13)$$

where

$$\begin{aligned} K^{KS}_{rs,\,tq} &= K^{KS}_{rs,\,tq} + K^{KS,XC}_{rs,\,tq} \\ &= \int \psi^*_r(1)\psi_s(1)\frac{1}{r_{12}}\psi^*_t(2)\psi_q(2)\mathrm{d}\tau_1\mathrm{d}\tau_2 \\ &\quad + \int \psi^*_r(1)\psi_s(1)f_{XC}[\rho^0,s^0]\psi^*_t(1)\psi_q(1)\mathrm{d}\tau_1 \end{aligned} \qquad (14)$$

In eq 14 $f_{XC}[\rho^0,s^0]$ represents the exchange−correlation kernel evaluated at the reference state with density ρ^0 and spin density s^0. It can be expressed[21,22] in terms of the functional derivatives of the exchange−correlation potential V_{XC} given in eq 6 with respect to the density ρ and spin s.

The CV-DFT[23] method considers an excitation as a perturbation of the reference system in which a single electron is moved from the space of the occupied orbitals, represented by $\Delta\rho_{occ} = -\Sigma_i^{occ}\Sigma_k^{occ}\Sigma_a^{vir}U^*_{ak}U_{ai}\psi^*_i(1)\psi_k(1')$ in eq 11, to the virtual space, represented by $\Delta\rho_{vir} = \Sigma_a^{vir}\Sigma_b^{vir}\Sigma_i^{occ}U^*_{ai}U_{bi}\psi^*_a(1)\psi_b(1')$ of eq 11. The total charge of $\Delta\rho_{occ}$ is readily found by integration to be $-\Sigma_i^{occ}\Sigma_a^{vir}U^*_{ai}U_{ai}$, whereas the total charge of $\Delta\rho_{vir}$ is $\Sigma_a^{vir}\Sigma_i^{occ}U^*_{ai}U_{ai}$. We now identify excited states with stationary points on $E_{KS}[\rho^0 + \Delta\rho'] - E_{KS}[\rho^0]$ for which $\Sigma_a^{vir}\Sigma_i^{occ}U^*_{ai}U_{ai} = \mathbf{U^t\cdot U} = 1$.

An optimization of $E_{KS}[\rho^0 + \Delta\rho'] - E_{KS}[\rho^0]$ from eq 12 with respect to U under the constraint $\mathbf{U^t\cdot U} = 1$ affords[23] the eigenvalue equation:

$$(A^{KS} + B^{KS})U^{(I)} = \lambda^{(I)}U^{(I)} \qquad (15)$$

Here $\lambda^{(I)}$ is the transition energy for the excited state I and $U^{(I)}$ is the corresponding optimized set of U_{ai} coefficients. Within the Tamm−Dancoff approximation[30] $B^{KS}_{ai,bj} = 0$ so that eq 15 can be rewritten as

$$A^{KS}U^{(I)} = \lambda^{(I)}U^{(I)} \qquad (16)$$

The eigenvalue eq 16 is identical to that obtained from TDDFT[21,22] in the adiabatic formulation after invoking the Tamm−Dancoff approximation.[30] However, in TDDFT the reference Ψ^0 must be[21,22] the ground state, whereas Ψ^0 in CV-DFT[23] can be any state that can be represented to zeroth order by a single Slater determinant. In deriving eqs 15 and 16 it was assumed that the set of spin orbitals $\{\psi_p(1); p = 1,\mathrm{occ} + \mathrm{vir}\}$ are solutions to eq 4. However this condition does not need to be satisfied. If the condition is not satisfied, then

$$A^{KS}_{ai,\,bj} = -\delta_{ab}F^{KS}_{ij} + \delta_{ij}F^{KS}_{ab} + F^{KS}_{ai,\,bj}; B^{KS}_{ai,\,bj} = K^{KS}_{ai,\,jb} \qquad (17)$$

Here F^{KS}_{rs} was defined in eq 7. Note that the operator $\hat{F}^{KS}(1)$ is defined with respect to the density ρ^0 and spin density S^0 evaluated from Ψ^0 using the unoptimized orbital set $\{\psi_i(1); i = 1,\mathrm{occ}\}$ that defines the determinant. As the energy in eq 12 is evaluated only to second order in U we refer[23] to our scheme as second-order CV-DFT [CV(2)-DFT]. We shall shortly return to the application of CV(2)-DFT to our two model systems.

Computational Parameters. The two models used in the present study are shown in Figures 1a and 2a, respectively. They were derived from the X-ray structures[1,2] of $[Cu_3(L)(\mu_3{-}O)]^{4+}$ and $[(DBED)_3Cu_3(\mu{-}OH)_3]^{3+}$. We shall refer to them as μ_3O and TrisOH, respectively, for consistency with other available experimental and theoretical studies on these systems.[3−5,13] Each copper atom in μ_3O is coordinated to five ligands in a distorted trigonal bipyramidal geometry.[1,3] The three copper atoms are bridged through a central oxygen atom. The initial X-ray structure has C_3 symmetry. TrisOH features three copper atoms, each coordinated with four ligands in a distorted tetrahedral configuration.[2,4] The connection between the copper atoms is

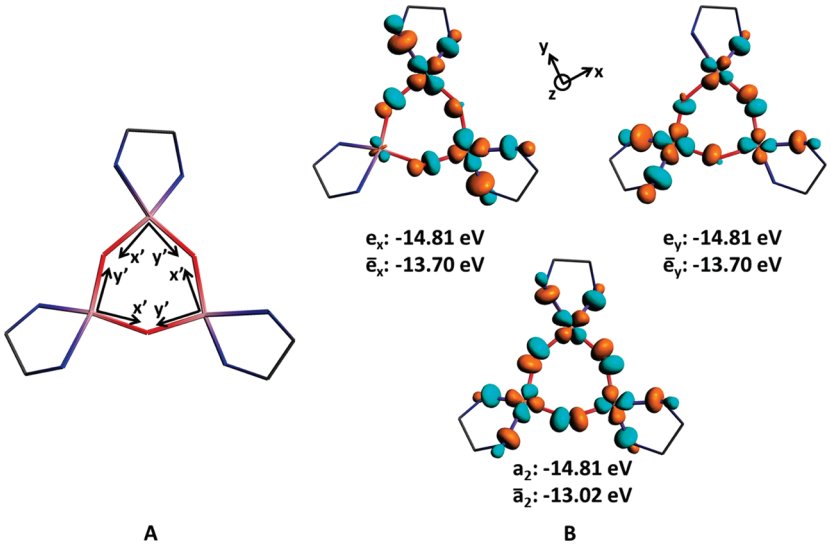

Figure 2. (A) Side view of the TrisOH model in D_3 symmetry. Included are the copper centered coordinate systems x',y',z'. (B) Frontier SUMO orbitals of $(TrisOH)_{D_3}$. Up: Front view of the $\bar{e}_x$ and $\bar{e}_y$ orbitals with the orbital energies and the orientation of the molecular coordinate system x,y,z. Down: Front and side view of $\bar{a}_2$, along with the values of the orbital energies. The SOMO orbitals a_2, e_x, and e_y are not shown, since they have similar spatial distribution as their SUMO counterparts.

made through three OH bridges which results in a planar hexagonal Cu_3O_3 structure. The ethylene bridges between the equatorial and axial N atoms in the μ_3O structure were truncated with H atoms reducing the size of the model to 58 atoms. In the TrisOH structure, a 45 atom model was created by replacement of the bulky tert-butyl groups by H atoms. The models on Figures 1a and 2a were optimized in C_{3v} and D_3 symmetry (see below) for μ_3O and TrisOH, respectively, with the C_3 axis perpendicular to the plane of the three copper atoms.

All calculations were based on the KS formalism,[19] as implemented in ADF (version 2009)[28,29] employing an all-electron TZ2P basis set. Geometry optimizations of the quartet reference states (see below for more details) were done in C_{3v} for μ_3O (configurations $a_1^1e_x^1e_y^1$) and D_3 for TrisOH (configurations $e_x^1e_y^1a_2^1$) using the regular unrestricted KS formalism.[19] Additional restricted KS-DFT calculations were carried out for a given geometry on the quartet reference states with occupation of 0.5 electrons assigned to the six orbitals which are in the original quartet reference state, the highest-occupied α- and the lowest-unoccupied β-molecular orbitals.

The calculations presented here made use of the following functionals: local density approximation Vosko−Wilk−Nusair (LDA-VWN),[31] BP86,[32,33] Becke−Lee−Yang−Parr (BLYP),[32−34] Perdew, Burke and Ernzerhof (PBE)[35] B3LYP,[36] and BHandHLYP.[36] The microstates for the two models in the different symmetries were generated with the clebeschgordan.exe program, written by M. A. Buijse.[37]

3. RESULTS AND DISCUSSION

Electronic Structure of μ_3O. Figures 1b and 2b display the frontier orbitals of μ_3O and TrisOH with their respective energies based on unrestricted DFT calculations using the LDA-VWN[31] functional. The quartet reference state has three unpaired electrons of α-spin in the a_1 and e orbitals for $(\mu_3O)_{C_{3v}}$ and in the a_2 and e orbitals for $(TrisOH)_{D_3}$. We shall refer to these orbitals as singly occupied molecular orbitals (SOMO's). The three lowest vacant orbitals have β-spin, and we shall refer to them as singly unoccupied molecular orbitals (SUMO's). The SUMO's have roughly the same composition as their SOMO counterparts but are higher in energy as the smaller number of β-electrons leads to fewer stabilizing exchange interactions for electrons of β-spin. In the description of the orbitals we shall make use of the local copper-centered coordinate axes x',y',z' (Figures 1a and 2a) introduced in ref 5.

The lowest SOMO and SUMO of $(\mu_3O)_{C_{3v}}$ are of a_1 symmetry. They feature a pseudo σ-antibonding interaction between the copper $d_{z'^2}$ orbitals and the p_z orbital of the central oxygen atom. This interaction appears upon a displacement of the oxygen atom above the plane of the three copper atoms. If the oxygen lies in the Cu_3 plane, then the overlap between these two sets of orbitals ceases. The position of the oxygen with respect to the plane of the metal atoms has been previously discussed in connection with the magnetic behavior of the μ_3O complex.[1,3,5] The vanishing overlap between the metal $d_{z'^2}$ orbitals and the oxygen p_Z orbital when the O atom is positioned in the Cu_3 plane leads to a decrease of the energy of the a_1 orbital, which increases the e−a_1 energy gap. As a consequence the out-of-plane conformation might be ferromagnetic with a $a_1^1e^2$ configuration (see below), whereas the in-plane conformation potentially could be antiferromagnetic with a $a_1^2e^1$ configuration.[1,3,5]

The doubly degenerate SOMO and SUMO of e symmetry are of higher energy than the corresponding a_1 orbitals due to the larger σ-antibonding overlap between the $d_{z'^2}$ orbitals of three or two copper atoms and the p_x or p_y orbitals of the oxygen. The motion of the O atom into the Cu_3 plane increases the antibonding interactions between the metal and oxygen orbitals leading to a higher energy of the e orbitals and a larger e−a_1 energy gap.

The three unpaired electrons in $(\mu_3O)_{C_{3v}}$ can be distributed within the six frontier spin orbitals to afford three possible electron configurations: $a_1^2e^1$, $a_1^1e^2$, and e^3. In addition, each of these configurations can give rise to microstates of different multiplicity and symmetry.

The construction of the symmetrized microstates is done with the clebeschgordan.exe program.[37] The number of the

Table 1. Doublet Microstates for μ_2O in C_{2v} Symmetry

C_{3v} microstates	M_s	C_{3v} symmetrized microstate functions
	$(a_1)^2e^1$ Configuration[a,b]	
$a(^2E_x)$	1/2	$\|a_1\bar{a}_1e_x\|$
	−1/2	$\|a_1\bar{a}_1\bar{e}_x\|$
$a(^2E_y)$	1/2	$\|a_1\bar{a}_1e_y\|$
	−1/2	$\|a_1\bar{a}_1\bar{e}_y\|$
	$(a_1)^1e^2$ Configuration	
$a(^2A_1)$	1/2	$1/\sqrt{2}(\|a_1e_x\bar{e}_x\| + \|a_1e_y\bar{e}_y\|)$
	−1/2	$1/\sqrt{2}(\|\bar{a}_1e_x\bar{e}_x\| + \|\bar{a}_1e_y\bar{e}_y\|)$
$a(^2A_2)$	1/2	$1/\sqrt{6}(-2\|\bar{a}_1e_xe_y\| + \|a_1\bar{e}_xe_y\| + \|a_1e_x\bar{e}_y\|)$
	−1/2	$1/\sqrt{6}(2\|a_1\bar{e}_x\bar{e}_y\| - \|\bar{a}_1\bar{e}_xe_y\| - \|\bar{a}_1e_x\bar{e}_y\|)$
$b(^2E_x)$	1/2	$1/\sqrt{2}(\|a_1e_x\bar{e}_x\| - \|a_1e_y\bar{e}_y\|)$
	−1/2	$1/\sqrt{2}(\|\bar{a}_1e_x\bar{e}_x\| - \|\bar{a}_1e_y\bar{e}_y\|)$
$b(^2E_y)$	1/2	$1/\sqrt{2}(-\|a_1e_x\bar{e}_y\| + \|a_1\bar{e}_xe_y\|)$
	−1/2	$1/\sqrt{2}(-\|\bar{a}_1e_y\bar{e}_y\| + \|\bar{a}_1\bar{e}_xe_y\|)$
	e^3 Configuration	
$c(^2E_x)$	1/2	$\|e_xe_y\bar{e}_y\|$
	−1/2	$\|\bar{e}_xe_y\bar{e}_y\|$
$c(^2E_y)$	1/2	$\|e_x\bar{e}_xe_y\|$
	−1/2	$\|e_x\bar{e}_x\bar{e}_y\|$

[a] Electron configuration. [b] a_1,e_x,e_y are the frontier orbitals of α-spin, whereas $\bar{a}_1$,$\bar{e}_x$,$\bar{e}_y$ are the frontier orbitals of β-spin.

Table 2. Quartet microstates for μ_3O in C_{3v} symmetry

C_{3v} microstates	M_s	C_{3v} symmetrized microstate functions
	$(a_1)^1e^2$ Configuration[a,b]	
$a(^4A_2)$	3/2	$\|a_1e_xe_y\|$
	1/2	$1/\sqrt{3}(\|a_1e_x\bar{e}_y\| + \|a_1\bar{e}_xe_y\| + \|\bar{a}_1e_xe_y\|)$
	−1/2	$1/\sqrt{3}(\|a_1\bar{e}_x\bar{e}_y\| + \|1e_x\bar{e}_y\| + \|\bar{a}_1\bar{e}_xe_y\|)$
	−3/2	$\|\bar{a}_1\bar{e}_x\bar{e}_y\|$

[a] Electron configuration. [b] a_1,e_x,e_y are the frontier orbitals of α-spin, whereas $\bar{a}_1$,$\bar{e}_x$,$\bar{e}_y$ are the frontier orbitals of β-spin.

microstates is calculated from combinatorics to be 20 of which many are degenerate. Tables 1 and 2 display all 20 doublet and quartet microstates which can be built with the 3 unpaired electrons and the 6 frontier SOMO and SUMO of $(\mu_3O)_{C_{3v}}$. The overall symmetry of the microstates can be evaluated from group theory.[38]

Detailed Description of Spin−Flip CV-DFT as Applied to $(\mu_3O)_{C_{3v}}$. The high-spin quartet reference state which is a starting point in most of our SF-CV(2)-DFT calculations arises from the $a_1{}^1e^2$ configuration. It is labeled as $a(^4A_2)_{3/2}$ and has $M_s = 3/2$ (Table 2). All other microstates can be obtained from the reference state by replacing one or more of the orbitals a_1, e_x or e_y with $\bar{a}_1$, $\bar{e}_x$, or $\bar{e}_y$, where a_1, e_x, and e_y refer to the α−orbitals, while $\bar{a}_1$, $\bar{e}_x$, and $\bar{e}_y$ refer to the β-orbitals.

The energy of a certain basic single determinantal microstate $\Psi_{i\rightarrow a}$ relative to the reference Ψ^0 can by analogy to single excitation configuration interaction (CIS)[39] in wave function mechanics be identified in CV(2)-DFT (or TDDFT) with the diagonal elements of the **A** matrix in eqs 13 and 17 according to

$$A_{ai,ai} = \langle \Psi_{i\rightarrow a}|H^{KS}|\Psi_{i\rightarrow a}\rangle = \varepsilon_a - \varepsilon_i + K^{KS}_{ai,ai} \quad (18)$$

Here $\Psi_{i\rightarrow a}$ is a single determinantal wave function obtained from Ψ^0 after a promotion of an electron from one of the occupied reference orbitals (including the SOMO's) with energy ε_i to one of the unoccupied reference orbitals (including the SUMO's) with energy ε_a. Further $K^{KS}_{ai,aj}$ is the combination of two-electron coulomb and exchange−correlation integrals defined in eq 14.

It is possible in general[37] to make symmetrized microstates of all the basic determinants $\Psi_{i\rightarrow a}$ that span the irreducible representation of the point group for the molecule under investigation as it was done specifically for the first 20 states in Tables 1 and 2. In order to evaluate the energy of each symmetrized microstate, one needs the diagonal elements of eq 18 as well as the off-diagonal elements given by

$$A_{aibj} = \langle \Psi_{i\rightarrow a}|H^{KS}|\Psi_{j\rightarrow b}\rangle = K^{KS}_{ai,bj} \quad (19)$$

in analogy to the single excitation CIS[39] in wave function mechanics.

It is now possible to determine the energy of all the doublet states with $M_s = 1/2$ within the $a_1^2e^1$, $a_1^1e^2$, and e^3 configurations relative to the $(^4A_2)_{3/2}$ reference by solving an eigenvalue equation $AU = \lambda U$ similar to that of eq 16. Here

$$A_{IJ} = \langle \Psi_I|H^{KS}|\Psi_J\rangle \quad (20)$$

are matrix elements between symmetrized microstates of the same representation. These states (I,J) include not only those doublet states with $M_s = 1/2$ within the $a_1^2e_1$, $a_1^1e^2$, and e^3 configurations, but all other $M_s = 1/2$ doublets generated by a spin−flip replacement of an occupied $(^4A_2)_{3/2}$ reference orbital ψ_i with a virtual reference orbital ψ_a. The elements in eq 20 can all be calculated based on eqs 18 and 19. The construction of A_{IJ} in eq 20 corresponds to a symmetry blocking[40] in space and spin of $A_{ai,bj}$ over all basic microstates.

It should be noted that a and i, as well as b and j, in eqs 18 and 19 are of different spins as all $M_s = 3/2$ doublets are generated from $(^4A_2)_{1/2}$ by a spin−flip $(i\rightarrow\bar{a})$, where i is of α-spin and $\bar{a}$ is of β-spin. The formulas for $K^{KS}_{\bar{a}i,\bar{b}j}$ required to evaluate eqs 18 and 19 were first derived in 2004 by Wang and Ziegler[25−27] based on a noncollinear exchange−correlation expression, see also refs 41 and 42. The same integrals would be zero in the collinear exchange−correlation formulation. We have

$$K^{KS,XC}_{\bar{a}i,\bar{b}j} = \int [\bar{\psi}_a{}^*(\vec{r}_1)\psi_i(\vec{r}_1)\bar{\psi}_b(\vec{r}_1)\psi_j^*(\vec{r}_1)] \left[\left(\frac{1}{s^0}\left(\frac{\partial E^{KS}_{XC}}{\partial\rho\alpha} - \frac{\partial E^{KS}_{XC}}{\partial\rho\beta}\right)\right)_{(\rho^0,s^0)}\right] d\vec{r}_1 \quad (21)$$

where integration over spin already has taken place so that $\bar{\psi}^*_a(\vec{r}_1)$ and $\bar{\psi}_b(\vec{r}_1)$ represent the spatial part of the two virtual orbitals of β-spin. The evaluation of $K^{KS,XC}_{\bar{a}i,\bar{b}j}$ by numerical integration might lead to numerical instabilities if $s^0 = \rho^\alpha - \rho^\beta \approx 0$. We can in that case carry out a Taylor expansion of $\partial E^{KS}_{XC}/\partial\rho_\alpha$ and $\partial E^{KS}_{XC}/\partial\rho^\beta$ from $\rho = \rho^\alpha + \rho^\beta = \rho^0$ and $s = 0$. Thus

$$\begin{aligned} K^{KS,XC}_{\bar{a}i,\bar{b}j} &= \int [\bar{\psi}_a{}^*(\vec{r}_1)\psi_i(\vec{r}_1)\bar{\psi}_b(\vec{r}_1)\psi_j^*(\vec{r}_1)] \\ &\approx \left[\left(\frac{\partial^2 E^{KS}_{XC}}{\partial\rho_\alpha^2} + \frac{\partial^2 E^{KS}_{XC}}{\partial\rho_\beta^2} - 2\frac{\partial^2 E^{KS}_{XC}}{\partial\rho_\alpha\partial\rho_\beta}\right)_{(\rho^0,s=0)}\right] d\vec{r}_1 \\ &= K^{KS,XC}_{ai,bj} - K^{KS,XC}_{ab,\bar{i}\bar{j}} \end{aligned} \quad (22)$$

Table 3. Lower Excited States for μ_3O of C_{3v} Symmetry Based on SF-CV(2)-DFT Calculations[a]

	C_{3v} symmetry[b]		
state	E, cm^{-1}	contributing microstates[c]	%
$1(^2E_{x,y})$	863[d] (645)[e]	$a(^2E_{x,y})$	70 (69)[e]
		$b(^2E_{x,y})$	18 (18)[e]
$2(^2E_{x,y})$	4630[d] (4533)[e]	$b(^2E_{x,y})$	74 (74)[e]
		$a(^2E_{x,y})$	23 (24)[e]
$1(^2A_1)$	5275[d] (5167)[e]	$a(^2A_2)$	100 (100)[e]
$1(^2A_2)$	6525[d] (6462)[e]	$a(^2A_1)$	100 (100)[e]
$3(^2E_{x,y})$	7985[d] (7929)[e]	$c(^2E_{x,y})$	87 (87)[e]

[a] LDA calculations. [b] LDA SF-CV(2)-DFT calculations carried out with C_{3v} symmetry and based on a $(\mu_3O)_{C_{3v}}$ geometry optimized for the $a(^4A_2)_{3/2}$ microstate using unrestricted KS-DFT. [c] Microstates defined in Tables 1 and 2. [d] Unrestricted calculations ($E[(\text{State})] - E[(^4A_2)_{3/2}]$) with orbitals optimized for $(^4A_2)_{3/2}$, relative to $(^4A_2)_{3/2}$ reference. [e] Restricted calculations ($E[(\text{State})] - E[(^4A_2)_{1/2}]$) with orbitals optimized from average configuration with 0.5 electrons in e_x, e_y, a_1, $\bar{e}_x$, $\bar{e}_y$, $\bar{a}_1$, relative to $(^4A_2)_{3/2}$ reference.

where $K^{KS,XC}_{ai,bj}$, $K^{KS,XC}_{ab,ij}$ are well-defined integrals from regular TDDFT.[21,22] The expression in eq 22 is correct to $(s^0)^3$ and has no singularities for $s^0 \approx 0$. It can thus be used for small values of s^0 where eq 21 becomes singular. In practice we have found that eq 21 can be used for the LDA-VWN[31] functional. For functionals based on the generalized gradient approximation (GGA), such as BP86,[32,33] BLYP,[32−34] and PBE,[35] where we can write the exchange−correlation energy as $E^{GGA}_{XC} = E^{LDA}_{XC} + \Delta E^{GGA}_{XC}$, we calculate the contribution from E^{LDA}_{XC} according to eq 21 and the contribution from ΔE^{GGA}_{XC} according to eq 22. For the hybrid functionals B3LYP[36] and BHandHLYP[36] we need in addition to calculate the regular exchange integrals

$$K^{HF,XC}_{\bar{a}i,\bar{b}j} = \iint \vec{\psi}^*_a(\vec{r}_1)\psi_i(\vec{r}_2)(1/r_{12})\vec{\psi}_b(\vec{r}_1)\psi^*_j(\vec{r}_2)d\vec{r}_1 d\vec{r}_2$$

already implemented in ADF.[43]

Results from SF-CV(2)-DFT Calculations on $(\mu_3O)_{C_{3v}}$. By solving the eigenvalue equation $A_\Gamma U^{(I)}_\Gamma = \lambda^{(I)}_\Gamma U^{(I)}_\Gamma$ for each symmetry representation Γ, where A_Γ is defined in eq 20, we obtain the state functions:

$$\Phi^{(I)}_\Gamma = \sum_q U^{(I)}_{\Gamma,q}\Psi_{\Gamma,q} \qquad (23)$$

as a linear combination of symmetrized microstates summed over q as well as the energies $\lambda^{(I)}_\Gamma$ relative to $(^4A_2)_{3/2}$. Table 3 presents $\lambda^{(I)}_\Gamma$ for the lowest doublet states with $M_s = 1/2$ based on SF-CV(2)-DFT calculations. In Table 3 is included also for each excited state I the participating microstates $\Psi_{\Gamma,q}$ with their percent contribution to $\Phi^{(I)}_\Gamma$ of eq 23. Some of the contributions are close to 100% which is indicative of a predominance of a certain symmetrized microstate in each excited state. However, in principle $\Phi^{(I)}_\Gamma$ can have contributions from the microstates of Table 1 and from all the microstates used to construct A_Γ of eq 20.

Table 3 displays results from restricted and unrestricted LDA SF-CV(2)-DFT calculations based on the unrestricted LDA KS-DFT geometries of the reference states $a(^4A_2)_{3/2}$ optimized with C_{3v} constraints. Here the unrestricted calculations make use of orbitals optimized for $a(^4A_2)_{3/2}$, whereas the restricted calculations employ orbitals from a SCF calculations in which a_1, e_x, e_y, $\bar{a}_1$, $\bar{e}_x$, and $\bar{e}_y$ each are assigned half an electron. The first real excited doublet is the doubly degenerate $1(^2E_{x,y})$ state. It is due to coupling of the $a(^2E_{x,y})$ and $b(^2E_{x,y})$ microstates with significant predominance of $a(^2E_{x,y})$. The complementary coupling with predominance of the $b(^2E_{x,y})$ microstates from the $a_1^1e^2$ configuration gives rise to excited state $2(^2E_{x,y})$ which is of higher energy. This result corresponds to the qualitative conclusions drawn for the microstates on the basis of the orbital energies (eq 18) with $a_1^2e^1$ below $a_1^1e^2$, with the exception of the ground state $(^4A_2)_{3/2}$ which also belongs to the electron configuration $a_1^1e^2$.

The following two excited states $1(^2A_1)$ and $1(^2A_2)$ are based solely on the $a(^2A_2)$ and $a(^2A_1)$ microstates, respectively. They originate from the same $a_1^1e^2$ configuration as $2(^2E_{x,y})$. The last spin−flip excitation of Table 3 yields a doublet degenerate $3(^2E_{x,y})$ state with a large contribution from the $c(^2E_{x,y})$microstate, consistent with the analysis based on the orbital energies.

The positive values in Table 3 for the energies $\lambda^{(I)}_\Gamma$ of the $M_s = 1/2$ doublets mean that these states are all above the $(^4A_2)_{3/2}$ reference. This is in line with experiment[1,3] that finds $(\mu_3O)_{C_{3v}}$ to have a ^4A ground state. The $(\mu_3O)_{C_{3v}}$ system is seen to favor for its ground state the high-spin quartet configuration $a_1^1e^2$ stabilized by extra exchange interaction integrals K^{KS} but having two electrons in e of high energy, instead of the low-spin doublet configuration $a_1^2e^1$ with two electrons paired on a_1 of low energy.

It is also in agreement with experiment that our calculations find a low lying $1(^2E_{x,y})$ excited state for $(\mu_3O)_{C_{3v}}$. This state is (based on magnetization experiments)[1,3] situated at $\Delta E = 163.5$ cm^{-1} above $^4A_2$. We find ΔE from our LDA SF-TDDFT calculations to be somewhat higher with $\Delta E = 863$ cm^{-1} for the unrestricted case (where $\Delta E = E[(^2E_{x,y})] - E[(^4A_2)_{3/2}]$, see below) and $\Delta E = 645$ cm^{-1} for the restricted case (where $\Delta E = E[(^2E_{x,y})] - E[(^4A_2)_{1/2}]$). In general the $\lambda^{(I)}_\Gamma$ values of Table 3 are slightly larger for the unrestricted results compared to the restricted SF-TDDFT numbers. This is understandable since the orbitals for the unrestricted calculations are optimized with respect to the $(^4A_2)_{3/2}$ reference with three electrons in a_1, e_x, and e_y, respectively, whereas the restricted calculations make use of orbitals from an averaged configuration with 1/2 electron in each of the orbitals a_1, e_x, e_y, $\bar{a}_1$, $\bar{e}_x$, and $\bar{e}_y$.

The energies in Table 3 were all based on the simple LDA[31] functional. We shall next examine how the energy difference ΔE between the lowest $^4A_2$ and $1(^2E_{x,y})$ states depends on the choice of functional. The difference ΔE is a key parameter and, as mentioned already, has been measured. It can be related directly to the exchange coupling constants J of the Heisenberg Hamiltonian[5,18,44] as $\Delta E = 3J$. Here $|J|$ is a measure of the strength of the coupling between spins of weakly interacting electrons on different metal centers. Further, $J < 0$ indicates antiferromagnetic coupling with a low-spin ground state, whereas $J > 0$ correspond to ferromagnetic coupling with a high-spin ground state.

We shall in the following determine ΔE as

$$\Delta E = E[(^2E_{X,Y})] - E[(^4A_2)_{1/2}] \qquad (24)$$

where both $E[(^2E_{x,y})]$ and $E[(^4A_2)_{1/2}]$ are found from SF-CV(2)-DFT calculations with $(^4A_2)_{3/2}$ as the reference. We have adopted eq 24 as it gives a more balanced description where both states are described on the same footing as opposed to the definition $\Delta E = E[(^2E_{x,y})] - E[(^4A_2)_{3/2}]$, where one state $(^4A_2)_{3/2}$ is described by a single determinant and the other $(^2E_{x,y})$ by SF-CV(2)-DFT (Table 3). Such a practice is common in studies based on multiconfiguration wave function theory.[45]

Table 4. Calculated[a] Energy Difference $\Delta E^{b,c}$ in $(\mu_3O)_{C3v}$ between Lowest Quartet State $(^4A_2)_{1/2}$ and Doublet State $(^2E_{x,y})_{1/2}$ for Different Functionals and Methods

	broken[d] symmetry	unrestricted[e,g] SF-CV(2)-DFT	restricted[f,g] SF-CV(2)-DFT
functionals	ΔE^d	ΔE^b	ΔE^b
LDA	879	664	645
BP86	617	468	365
BLYP	561	414	334
PBE	613	465	363
B3LYP	471	385	318
BHandHLYP	134	142	152

[a] Based on geometry optimized for $(^4A_2)_{3/2}$. [b] $E[(^2E_{x,y})] - E[(^4A_2)_{1/2}]$. [c] In cm^{-1}. [d] Calculated according to ref 5 as $\Delta E = E(LS) - E[(^4A_1)_{3/2}] = 3J = (3/2)\{E(BS) - E[(^4A_1)_{3/2}]\}$, where $E(BS)$ is the energy from a broken symmetry calculation.[5,18,44] [e] Unrestricted calculations with orbitals optimized for $(^4A_2)_{3/2}$. [f] Restricted calculations with orbitals optimized from average configuration with 0.5 electrons in e_x, e_y, a_1, $\bar{e}_x$, $\bar{e}_y$, $\bar{a}_1$. [g] Relative to $(^4A_2)_{3/2}$ reference.

Table 5. Doublet Microstates for TrisOH in D_3 Symmetry

D_3 microstates	M_s	D_3 symmetrized microstate functions
	e^3 Configuration[a,b]	
$a(^2E_x)$	1/2	$\lvert e_x e_y \bar{e}_y\rvert$
	−1/2	$\lvert \bar{e}_x e_y \bar{e}_y\rvert$
$a(^2E_y)$	1/2	$\lvert e_x \bar{e}_x e_y\rvert$
	−1/2	$\lvert e_x \bar{e}_x \bar{e}_y\rvert$
	$e^2(a_2)^1$ Configuration	
$a(^2A_2)$	1/2	$1/\sqrt{2}(\lvert e_x \bar{e}_x a_2\rvert + \lvert e_y \bar{e}_y a_2\rvert)$
	−1/2	$1/\sqrt{2}(\lvert e_x \bar{e}_x \bar{a}_2\rvert + \lvert e_y \bar{e}_y \bar{a}_2\rvert)$
$a(^2A_1)$	1/2	$1/\sqrt{6}(2\lvert e_x e_y \bar{a}_2\rvert - \lvert e_y \bar{e}_y a_2\rvert - \lvert \bar{e}_x e_y a_2\rvert)$
	−1/2	$1/\sqrt{6}(-2\lvert \bar{e}_x \bar{e}_y a_2\rvert + \lvert e_y \bar{e}_y \bar{a}_2\rvert + \lvert \bar{e}_x e_y \bar{a}_2\rvert)$
$b(^2E_x)$	1/2	$1/\sqrt{2}(\lvert \bar{e}_x e_y a_2\rvert - \lvert e_x \bar{e}_y a_2\rvert)$
	−1/2	$1/\sqrt{2}(\lvert \bar{e}_x e_y \bar{a}_2\rvert - \lvert e_x \bar{e}_y \bar{a}_2\rvert)$
$b(^2E_y)$	1/2	$1/\sqrt{2}(\lvert e_y \bar{e}_y a_2\rvert - \lvert e_x \bar{e}_x a_2\rvert$
	−1/2	$1/\sqrt{2}(\lvert e_y \bar{e}_y \bar{a}_2\rvert - \lvert e_x \bar{e}_x \bar{a}_2\rvert)$
	$e^1(a_2)^2$ Configuration	
$c(^2E_x)$	1/2	$\lvert e_x a_2 \bar{a}_2\rvert$
	−1/2	$\lvert \bar{e}_x a_2 \bar{a}_2\rvert$
$c(^2E_y)$	1/2	$\lvert e_y a_2 \bar{a}_2\rvert$
	−1/2	$\lvert \bar{e}_y a_2 \bar{a}_2\rvert$

[a] Electron configuration. [b] a_2, e_x, e_y are the frontier orbitals of α-spin, whereas $\bar{a}_2, \bar{e}_x, \bar{e}_y$ are the frontier orbitals of β-spin.

Table 6. Quartet Microstates for TrisOH in D_3 Symmetry

D_3 microstates	M_s	D_3 symmetrized microstate functions
	$e^2(a_2)^1$[a,b]	
$a(^4A_1)$	3/2	$\lvert e_x e_y a_2\rvert$
	1/2	$1/\sqrt{3}(\lvert e_x e_y \bar{a}_2\rvert + \lvert e_x \bar{e}_y a_2\rvert + \lvert \bar{e}_x e_y a_2\rvert)$
	−1/2	$1/\sqrt{3}(\lvert e_x \bar{e}_y \bar{a}_2\rvert + \lvert \bar{e}_x \bar{e}_y a_2\rvert + \bar{e}_x e_y \bar{a}_2\rvert)$
	−3/2	$\lvert \bar{e}_x \bar{e}_y \bar{a}_2\rvert$

[a] Electron configuration. [b] a_2, e_x, e_y are the frontier orbitals of α-spin, whereas $\bar{a}_2, \bar{e}_x, \bar{e}_y$ are the frontier orbitals of β-spin.

It is also possible[5,18,44] to estimate ΔE within DFT by the "broken-symmetry approach" (BS), where one performs one high-spin calculation on $a_1^1e^2$ followed by one low-spin calculation in which the symmetry of a_1, e_x, and e_y is allowed to break by letting each of the orbitals localize on a different Cu center. It is possible to relate ΔE to the energy difference between the high- and low-spin calculations. We compare in Table 4 ΔE from BS calculations with those obtained by employing either the unrestricted or restricted SF-CV(2)-DFT method for different functionals.

We see in Table 4 that the calculated ΔE values have the same large dependence on the functionals for all three methods. Thus LDA[31] affords the largest estimate whereas the GGA (BP86,[32,33] BLYP,[32−34] PBE[35]) values for ΔE are close and intermediate. The two hybrids (B3LYP[36] and BHandHLYP)[36] give rise to the smallest values with ΔE(BHandHLYP) < ΔE(B3LYP) For LDA, the GGA's and B3LYP the ΔE values for the same functional tend to be somewhat larger (100−150 cm^{-1}) for the BS scheme than the SF-CV(2)-DFT methods. This gap might close somewhat if use is made of the more refined BS formulation due to Yamaguchi et al.[46] in which the overlap between the broken symmetry orbitals is taken into account. For LDA, the GGA's and B3LYP we find further that the restricted SF-CV(2)-DFT method affords ΔE values that on average are some 50 cm^{-1} smaller than the unrestricted estimates. The trend is what one would expect for reasons already mentioned. The margin is also an indication of the possible error for spin contamination present in the unrestricted scheme but not in the restricted method. We recommend the restricted SF-CV(2)-DFT method as the more accurate of the two SF-CV(2)-DFT schemes as it is free of spin contamination.

Chalupsky et al.[16] have in a recent high-level CASPT2 calculation obtained an estimate for ΔE of 165 cm^{-1} in very good agreement with the experimental value of 163.5 cm^{-1}. We obtain the best agreement for the BHandHLYP functional with values of 134 cm^{-1} (BS), 142 cm^{-1} (unrestricted SF-CV(2)-DFT), and 152 cm^{-1} (restricted SF-CV(2)-DFT), respectively. It is interesting to note that the BS scheme and the SF-CV(2)-DFT method, which appear very different, afford quite similar results especially for the BHandHLYP functional.

Electronic Structure and Ground-State Geometry of TrisOH. The frontier orbitals of TrisOH (Figure 2b) feature σ-antibonding interactions between the copper $d_{x'^2-y'^2}$ orbitals and p_x, p_y on oxygen. The a_2 orbital is the highest in energy since all six atoms of the planar Cu_3O_3 cycle are involved in the σ-antibonding overlap. The antibonding interaction is reduced in the e-set as it can be seen for e_x where it is confined to two copper and three oxygen atoms.

Similarly to $(\mu_3O)_{C_{3v}}$, $(TrisOH)_{D_3}$ has three different low-energy electron configurations, e^3, $e^2a_2^1$, and $e^1a_2^2$. The microstates corresponding to these configurations are shown in Tables 5 and 6. Their relative energies can be evaluated qualitatively from the orbital energies (eq 18). Microstates $a(^2E_x)$ and $a(^2E_y)$ arise from configuration e^3. They should be the doublet microstates of lowest energy. Configuration $e^2a_2^1$ contains the doublets $a(^2A_1)$, $a(^2A_2)$, and $b(^2E_{x,y})$, which are the microstates of intermediate energy. The sole quartet microstate $a(^4A_1)$ belongs to configuration $e^2a_2^1$ as well. The last electron configuration $e^1a_2^2$ affords the microstates $c(^2E_{x,y})$ of highest energy.

Results from SF-CV(2)-DFT Calculations on TrisOH. Table 7 displays the "restricted" and "unrestricted" LDA SF-TDDFT excitation energies for $(TrisOH)_{D_3}$ relative to the $(^4A_1)_{3/2}$ reference. Here the energy of $(^4A_1)_{3/2}$ has been obtained by optimizing both the orbitals and the geometry from high-spin unrestricted KS calculations based on the $a(^4A_1)_{3/2}$ microstate of Table 6. Further, all the LDA excited-state energies given in Table 7 are based on the optimized structure for $a(^4A_1)_{3/2}$. The lowest doubly degenerate excited state $[1(^2E_{x,y})]$ features coupling of microstates $a(^2E_{x,y})$ and $b(^2E_{x,y})$ with a significant predominance of $a(^2E_{x,y})$. The negative excitation energy in Table 7 is an indication that $1(^2E_{x,y})$ has in fact a lower energy than the reference quartet $a(^4A_1)_{3/2}$. It can thus be regarded as the ground state of the $(TrisOH)_{D_3}$ model. This is consistent with the experimental results according to which TrisOH has a ^2E ground state and a low-lying quartet excited state situated 315 cm^{-1} (ΔE = −315 cm^{-1}) above the ground state.[2,4] Our doublet−quartet splitting is however overestimated with ΔE = −2351 cm^{-1} for the unrestricted SF-CV(2)-DFT LDA calculation and ΔE = −2333 cm^{-1} for the restricted SF-CV(2)-DFT LDA calculation. The BS-DFT approach yields ΔE = −2783 cm^{-1} (Table 8).

The three states based on the $e^2a_2^1$ configuration $[2(^2E_{x,y})$, $1(^2A_1)$, and $1(^2A_2)]$ are as expected of higher energy than $1(^2E_{x,y})$. The state $2(^2E_{x,y})$ is a product of the coupling of microstates $b(^2E_{x,y})$ and $a(^2E_{x,y})$ with predominance of $b(^2E_{x,y})$, and $1(^2A_1)$ and $1(^2A_2)$ arise from microstates $a(^2A_1)$ and $a(^2A_2)$, respectively. A few states due to transitions between the SOMO's and virtual orbitals closely above the SUMO's or from occupied orbitals below the SOMO's to the SUMO's are found after $1(^2A_2)$ and are not presented in Table 7, since they do not belong to the discussed electron configurations. The last SOMO to SUMO excitation gives rise to state $4(^2E_{x,y})$ originating from the $e^1a_2^2$ electron configuration and microstates $c(^2E_{x,y})$.

We present in Table 8 values for $\Delta E = E[(^2E_{x,y})] - E[(^4A_1)_{1/2}]$ based on different functionals. The gap ΔE was calculated with both the unrestricted and restricted SF-CV(2)-DFT schemes using the same procedure as the one outlined earlier for μ_3O. Also shown are estimates due to the BS method. We find for LDA and the GGA's that ΔE in absolute terms is somewhat larger for the BS scheme compared to the unrestricted SF-CV(2)-DFT method. Most likely some of the discrepancy can be reduced by the Yamaguchi correction[46] not available in the ADF program. In going from the unrestricted to the restricted estimates for ΔE we encounter as expected for LDA, the GGA's and B3LYP a reduction in the gap. The CASPT2 method[16] affords for $(TrisOH)_{D_3}$ a value of −196 cm^{-1} for ΔE compared to the experimental estimate[2,4] of ΔE = −315 cm^{-1}. Our BHandHLYP results come close to the experimental value with −249 cm^{-1} (BS), −239 cm^{-1} (unrestricted), and −284 cm^{-1} (restricted). Thus as for μ_3O, BHandHLYP affords for all three methods the closest fit with experiment in the case of TrisOH.

Table 7. Lower Excited States for TrisOH in D_3 Symmetry Based on SF-TDDFT Calculations[a]

D_3 symmetry[b]			
state	E, cm^{-1}	contributing microstates[c]	%
$1(^2E_{x,y})$	−2315[d] (−2333)[e]	$a(^2E_{x,y})$	86(85)[e]
		$b(^2E_{x,y})$	8(9)[e]
$2(^2E_{x,y})$	4815[d] (4790)[e]	$b(^2E_{x,y})$	86(84)[e]
		$a(^2E_{x,y})$	11(12)[e]
$1(^2A_1)$	6686[d] (6733)[e]	$a(^2A_1)$	100(100)[e]
$1(^2A_2)$	6791[d] (6868)[e]	$a(^2A_2)$	100(100)[e]
$4(^2E_{x,y})$	11 042[d] (11 061)[e]	$c(^2E_y)$	87(79)[e]

[a] LDA calculations. [b] LDA SF-TDDFT calculations carried out with D_3 symmetry and based on a (TrisOH) geometry optimized for the $a(^4A_1)_{3/2}$ microstate. [c] Microstates defined in Tables 5 and 6. [d] Unrestricted calculations ($E[(State)] - E[(^4A_1)_{3/2}]$) with orbitals optimized for $(^4A_1)_{3/2}$, relative to $(^4A_1)_{3/2}$ reference. [e] Restricted calculations ($E[(State)] - E[(^4A_1)_{1/2}]$) with orbitals optimized from average configuration with 0.5 electrons in e_x, e_y, a_2, $\bar{e}_x$, $\bar{e}_y$, $\bar{a}_2$, relative to $(^4A_1)_{3/2}$ reference.

Table 8. Calculated[a] Energy Difference ΔE[b,c] in TrisOH between Lowest Quartet State $(^4A_1)_{1/2}$ and Doublet State $(^2E_{x,y})_{1/2}$ for Different Functionals and Methods

	Broken[d] Symmetry	Unrestricted[e,g] SF-CV(2)-DFT	Restricted[f,g] SF-CV(2)-DFT
functionals	ΔE[d]	ΔE[b]	ΔE[b]
LDA	−2783	−2463	−2333
BP86	−2074	−1951	−1826
BLYP	−2082	−1948	−1824
PBE	−2094	−1968	−1840
B3LYP	−720	−721	−572
BHandHLYP	−249	−239	−284

[a] Based on geometry optimized for $(^4A_1)_{3/2}$. [b] $E[(^2E_{x,y})] - E[(^4A_1)_{1/2}]$. [c] In cm^{-1}. [d] Calculated according to ref 5 as $\Delta E = E(LS) - E[(^4A_1)_{3/2}] = 3J = (3/2)\{E(BS) - E[(^4A_1)_{3/2}]\}$, where $E(BS)$ is the energy from a broken symmetry calculation.[5,18,44] [e] Unrestricted calculations with orbitals optimized for $(^4A_1)_{3/2}$. [f] Restricted calculations with orbitals optimized from average configuration with 0.5 electrons in e_x, e_y, a_2, $\bar{e}_x$, $\bar{e}_y$, $\bar{a}_2$. [g] Relative to $(^4A_1)_{3/2}$ reference.

4. CONCLUDING REMARKS

We have here applied the spin−flip formalism[24] in conjunction with the noncollinear exchange−correlation formulation[25−27,41,42] of CV(2)-DFT[23] to study spin−exchange and multiplet splittings in the two model systems $[Cu_3(L)(\mu_3{-}O)]^{4+}$ and $[(DBED)_3Cu_3(\mu{-}OH)_3]^{3+}$. We have shown that SF-CV(2)-DFT affords exchange coupling constants (J) that are similar to the values obtained by the broken-symmetry scheme due to Noodleman[18,44] and Yamaguchi[46] for a given functional. For the two systems at hand both BS-DFT and SF-CV(2)-DFT predict correctly that $[Cu_3(L)(\mu_3{-}O)]^{4+}$ is ferromagnetic, whereas the $[(DBED)_3Cu_3(\mu{-}OH)_3]^{3+}$ system is antiferromagnetic for all functionals. Both LDA and the GGA's overestimate in absolute terms the exchange coupling constants (J). On the other hand, the BHandHLYP functional affords estimates for both $[Cu_3(L)(\mu_3{-}O)]^{4+}$ and $[(DBED)_3Cu_3(\mu{-}OH)_3]^{3+}$ that are in good agreement with experiment[1−4] and high-level theory[16] in the case of BS-DFT as well as SF-CV(2)-DFT. More work has to be done to establish SF-CV(2)-DFT as an alternative to BS-DFT in the calculation of exchange coupling constants.

The SF-CV(2)-DFT method is not only able to evaluate exchange coupling constants, it can in addition calculate the full multiplet spectrum with complete use of spatial symmetry. Further, in its restricted formulation calculations can be carried out with use of full spin symmetry without spin contamination. Finally, SF-CV(2)-DFT can also be used to optimize[47] the geometry of each individual spin state, an option we plan to pursue in the near future. Our study adds to the increasing body of work based on DFT (or TDDFT) directed toward the study of spin multiplets[48,49] and weakly interacting spin systems.[50,51]

AUTHOR INFORMATION

Corresponding Author

*E-mail: ziegler@ucalgary.ca.

ACKNOWLEDGMENT

This work was supported by NSERC as well as a scholarship (H.Z.) from the University of Calgary. T.Z. thanks the Canadian Government for a Canada Research Chair.

REFERENCES

(1) Suh, M. P.; Han, M. Y.; Lee, J. H.; Min, S. K.; Hyeon, C. *J. Am. Chem. Soc.* **1998**, *120*, 3819–3820.
(2) Mirica, L. M.; Stack, T. D. P. *Inorg. Chem.* **2005**, *44*, 2131–2133.
(3) Yoon, J.; Solomon, E. I. *Inorg. Chem.* **2005**, *44*, 8076–8086.
(4) Yoon, J.; Mirica, L. M.; Stack, T. D. P.; Solomon, E. I. *J. Am. Chem. Soc.* **2004**, *126*, 12586–12595.
(5) Yoon, J.; Mirica, L. M.; Stack, T. D. P.; Solomon, E. I. *J. Am. Chem. Soc.* **2005**, *127*, 13680–13693.
(6) Solomon, E. I.; Augustine, A. J.; Yoon, J. *Dalton. Trans.* **2008**, 3921–3932.
(7) Solomon, E. I.; Sundaram, U. M.; Machonkin, T. E. *Chem. Rev.* **1996**, *96*, 2563–2605.
(8) Solomon, E. I.; Chen, P.; Metz, M.; Lee, S.-K.; Palmer, A. E. *Angew. Chem., Int. Ed.* **2001**, *40*, 4570–4590.
(9) Davies, G. J.; Ducros, V. In *Handbook of Metalloproteins*; Messerschmidt, A., Huber, R., Wieghardt, K., Poulos, T., Eds.; Wiley: New York, 2001; pp 1359.
(10) Malkin, R.; Malmström, B. G. *Adv. Enzymol.* **1970**, *33*, 177–&.
(11) Crichton, R. R.; Pierre, J.-L. *BioMetals* **2001**, *14*, 99–112.
(12) deSilva, D. M.; Askwith, C. C.; Eide, D.; Kaplan, J. *J. Biol. Chem.* **1995**, *270*, 1098–1101.
(13) Yoon, J.; Solomon, E. I. *Coord. Chem. Rev.* **2007**, *251*, 379–400.
(14) Andersson, K.; Malmqvist, P. A.; Roos, B. O.; Sadlej, A. J.; Wolinski, K. *J. Phys. Chem.* **1990**, *94*, 5483–5488.
(15) Roos, B. O.; Andersson, K.; Fulscher, M. P.; Malmqvist, P. A.; Serrano-Andres, L.; Pierloot, K.; Merchan, M. In *Advances in Chemical Physics: New Methods in Computational Quantum Mechanics*; Prigogine, I., Rice, S. A., Eds.; John Wiley & Sons: New York, 1996; Vol. XCIII, p 219.
(16) Chalupský, J.; Neese, F.; Solomon, E. I.; Ryde, U.; Rulíšek, L. *Inorg. Chem.* **2006**, *45*, 11051–11069.
(17) Vancoillie, S.; Chalupský, J.; Ryde, U.; Solomon, E. I.; Pierloot, K.; Neese, F.; Rulíšek, L. *J. Phys. Chem. B* **2010**, *114*, 7692–7702.
(18) Noodleman, L.; Case, D. A.; Aizman, A. *J. Am. Chem. Soc.* **1988**, *110*, 1001–1005.
(19) Koch, W.; Holthausen, M. C. *A Chemist's Guide to Density Functional Theory*, Wiley-VCH: New York, 2001.
(20) Sinn, E. *Coord. Chem. Rev.* **1970**, *5*, 313–347.
(21) Runge, E.; Gross, E. K. U. *Phys. Rev. Lett.* **1984**, *52*, 997–1000.
(22) Casida, M. E. In *Recent Advances in Density Functional Methods*; D. E. Chong, Ed.; World Scientific: Singapore, 1995; p 155.
(23) Ziegler, T.; Seth, M.; Krykunov, M.; Autschbach, J.; Wang, F. *J. Chem. Phys.* **2009**, *130*, 154102–(1−8).
(24) Krylov, A. *Acc. Chem. Res.* **2006**, *39*, 83–91.
(25) Wang, F.; Ziegler, T. *J. Chem. Phys.* **2004**, *121*, 12191–12196.
(26) Wang, F.; Ziegler, T. *J. Chem. Phys.* **2005**, *122*, 074109–(1−9).
(27) Wang, F.; Ziegler, T. *Int. J. Quantum Chem.* **2006**, *106*, 2545–2550.
(28) te Velde, G.; Bickelhaupt, F. M.; Baerends, E. J.; van Gisbergen, S. J. A.; Fonseca Guerra, C.; Snijders, J. G.; Ziegler, T. *J. Comput. Chem.* **2001**, *22*, 931–967.
(29) *ADF2009.01, SCM, Theoretical Chemistry*; Vrije Universiteit: Amsterdam, The Netherlands; http://www.scm.com.
(30) Hirata, S.; Head-Gordon, M. *Chem. Phys. Lett.* **1999**, *314*, 291–299.
(31) Vosko, S. H.; Wilk, L.; Nusair, M. *Can. J. Phys.* **1980**, *58*, 1200–1211.
(32) Becke, A. D. *Phys. Rev. A* **1988**, *38*, 3098–3100.
(33) Perdew, J. P.; Wang, Y. *Phys. Rev. B* **1986**, *33*, 8822–8824.
(34) Lee, C.; Yang, W.; Parr, R. G. *Phys. Rev. B* **1988**, *37*, 785–789.
(35) Perdew, J. P.; Burke, K.; Ernzerhof, M. *Phys. Rev. Lett.* **1996**, *77*, 3865–3868. **1997**, *78*, 1396–1396 (E).
(36) Becke, A. D. *J. Chem. Phys.* **1993**, *98*, 1372–1377.
(37) *Clebeschgordan.exe*; Buijse, M. A., University de Boelelaan: Amsterdam, The Netherlands,1991.
(38) Koster, F. G.; Dimmock, J. O.; Wheeler, R. G.; Statz, H. *Properties of the Thirty-Two Point Groups*; M.I.T. Press: Cambridge, Massachusets, 1963.
(39) Foresman, J. B.; Head-Gordon, M.; Pople, J. A.; Frisch, M. J. *J. Phys. Chem.* **1992**, *96*, 135–149.
(40) van Gisbergen, S. J. A.; Snijders, J. G.; Baerends, E. J. *Comput. Phys. Commun.* **1999**, *118*, 119–138.
(41) Wang, F.; Liu, W. *J. Chin. Chem. Soc. (Taipei)* **2003**, *50*, 597–606.
(42) Gao, J.; Liy, W.; Song, B.; Liu, C. *J. Chem. Phys.* **2004**, *121*, 6658–6666.
(43) Krykunov, M.; Ziegler, T.; van Lenthe, E. *J. Phys. Chem. A* **2009**, *113*, 11495–11500.
(44) Noodleman, L. *J. Chem. Phys.* **1981**, *74*, 5737–5743.
(45) Shavitt, I. In *Methods of Electronic Structure Theory*; Schaefer, H. F., III, Ed.; Plenum: New York, 1977; pp 189−275.
(46) Yamaguchi, K.; Jensen, F.; Dorigo, A.; Houk, K. N. *Chem. Phys. Lett.* **1988**, *149*, 537–542.
(47) Seth, M.; Mazur, G.; Ziegler, T. *Theor. Chem. Acc.* **2010**ASAP.
(48) Vahtras, O.; Rinkevicius, Z. *J. Chem. Phys.* **2007**, *126* (11), 114101–114111).
(49) Li, Z.; Liu, W. *J. Chem. Phys.* **2010**, *133* (06), 064106–064128).
(50) Rinkevicius, Z.; Ågren, H. *Chem. Phys. Lett.* **2010**, *491*, 132–135.
(51) Moreira, I. P. R; Sosta, R.; Filatov, M.; Illas, F. *J. Chem. Theory Comput.* **2007**, *3*, 764–774.